

Automatic Registration of Airborne Images by Combining Area-based Methods with Local Transformation Models

Desheng Liu

dsliu@nature.berkeley.edu

Department of Environmental Science, Policy and Management

University of California, Berkeley

Abstract

Image registration is a critical preprocessing procedure in many remote sensing applications, including multi-sensor image fusion, temporal change detection, and image mosaicking. Registration parameters for satellite imagery are usually modeled by global transformations, but registration of airborne images using global models often results in large errors due to complex local geometric distortion. To solve this problem, local transformation models such as piecewise mapping functions are often used to register airborne images. These models require large numbers of evenly distributed control points to represent local variation. Therefore, the quantity and spatial distribution of extracted control points are crucial to the registration accuracy of images with complex local deformation. In this paper, I propose a solution to the registration problem in two parts. First, I presented an area-based method to extract sufficient numbers of well-located control points, and second, I used the extracted control points with local transformation models to register multi-temporal airborne images. Two similarity metrics (correlation coefficient and mutual information) were compared for the control point extraction. Control points extracted from the area-based methods and manual selection were then applied with piecewise mapping functions and global polynomial functions to register multi-temporal airborne images. The new method achieved higher registration accuracy compared with the more conventional global transformation models and manual selection methods.

1. Introduction

Image registration is a critical preprocessing procedure in all remote sensing applications that utilize multiple image inputs, including multi-sensor image fusion, temporal change detection, and image mosaicking. With the recent explosive increase in remotely sensed imagery, and the corresponding interest in temporal change detection and modeling, automatic image registration has become increasingly important for the integration of multi-temporal and multi-sensor data (Moigne, 2002). Earth system science, for example, will increasingly rely on automated tools for the integration and registration of multi-temporal and multi-sensor satellite and airborne imagery as the necessary first step in the analysis of seasonal and annual global climate change and land use / land cover change (Townshend et al, 1992; Dai and Khorram, 1998). In addition, imagery acquired from aircraft (as opposed to satellites) often has additional spatial registration issues caused by sensor parameter changes from mission to mission (Coulter et al, 2003), making accurate image to image registration even more important.

The automatic registration of images has generated extensive research interests in the fields of computer vision, medical imaging and remote sensing. Comprehensive reviews include Brown (1992) and Zitova and Flusser (2003). Review on remote sensing applications can be found in

Fonseca and Manjunath (1996). Image registration is the process of geometrically aligning two or more images of the same scene. The method generally consists of four steps: 1) control point extraction, 2) transformation model determination, 3) image transformation and resampling, and 4) registration accuracy assessment (Jensen, 2004). Among the four steps, the first two are the most complex, and their success essentially determines the registration accuracy.

While many of the standard remote sensing texts discuss manual control point extraction (Schowengerdt, 1997), this method can be subjective and extremely time consuming, and often results in few usable points, with poor spatial distribution across the image, both of which can reduce the overall registration accuracy (Kennedy and Cohen, 2003). Automated extraction of control points is a solution to this problem, and is approached by either feature-based methods or area-based methods. Feature-based methods apply feature extraction algorithms to generate a certain number of obvious features first and then match these features to form the control point pairs. The commonly used features are landmarks (e.g. edges, corners, the centers of gravity of regions, and line intersections) extracted from the image. Feature-based methods are robust to intensity change and geometric distortion; however, they rely on the existence of robust features invariant between images and efficient feature extraction algorithms, which are not always easy to implement (Kennedy and Cohen, 2003). In addition, the possibility of too few or unevenly distributed features may limit their use in some applications (Chen et al, 2003). In contrast, area-based methods work with subset images directly without feature extraction and compare the similarity of sub-images within corresponding windows at different displacements. Area-based methods are usually computationally intensive and may not be applicable to image pairs with large rotational distortion, but they have the advantage of being relatively easy to implement and require no pre-processing of images. Moreover, the regular grid distribution of the resulting control points is often desirable for image registration, because sufficient numbers of control points can cover the complex local distortions that might be found across an image.

Transformation models used in image registration are either global transformations or local transformations depending on whether the transformation function is location dependent (Brown, 1992). The registration of satellite images is commonly modeled as a global deformation, but the local geometric distortion is not always negligible depending on the imaging geometry, the terrain variation, atmospheric turbulence and the sensor nonlinearity (Richards and Jia, 1999). In particular, airborne images with high spatial resolution often have complex local deformation caused by the wide view angle, the terrain variation, the low flight height, and the effects of yaw, pitch, and roll (Devereux, 1990). For complex local deformation, piecewise mapping functions (Goshtasby, 1986, 1987, 1988b) and surface spline mapping functions (Goshtasby, 1988a; Flusser, 1992) are often used as local transformation models. These models usually need large numbers of evenly distributed control points or features to represent the local variation. Therefore, the quantity and spatial distribution of extracted control points are crucial to the accuracy of the registration of images with complex local deformation.

Since feature-based control point extraction methods rely on the extraction and matching of prominent features to be the control points, these methods are not always capable of finding enough evenly distributed features as the control points for each local deformed region, especially for images that lack structures or patterns. In addition, feature extraction and matching are often difficult due to the dominance of ambiguous features. Although global matching

(Moigne, 2002) can solve this problem, this method is not applicable to the local transformation models. Consequently, feature-based control point extraction methods are not suitable for imagery with complex local deformation. In this regard, area-based methods become more appropriate in the selection of control points for the use of local transformation models since the control points can be evenly arranged on regular grids to represent the complex local distortion and the matching can be obtained by optimizing some similarity measures based on the gray value of images.

This paper focuses on the automatic registration of high spatial resolution airborne imagery with complex local deformation. Although a frame center matching technique can be employed during the acquisition of the airborne images to alleviate many of the complicating factors to image distortion (Coulter et al, 2003), it is still necessary to develop appropriate algorithms to account for complex local deformation for airborne imagery acquired without that technique. My objective is to apply area-based control point extraction algorithms together with local transformation models to the registration of multi-temporal airborne images. I also compared the results from automated control point extraction with simulated manual control point extraction methods.

2. Methods

2.1 Study Site and Data Description

The study site for this research is a forested peninsula on the east side of Marin County, CA, called China Camp State Park. The area has moderate to steep topography, with elevations ranging from sea level at San Pablo Bay (the northerly lobe of the San Francisco Bay) to over 300m. High spatial-resolution imagery has been collected for the area for four years, using an airborne ADAR 5500 (Airborne Data Acquisition and Registration) sensor. I present results in this paper for imagery from spring 2000 and 2001. The ADAR 5500 imaging system is comprised of a SN4, 20mm lens with four mounted cameras (spectral bands: band 1 (blue): 450-550nm, band 2 (green): 520-610nm, band 3 (red): 610-700nm, band 4 (near infrared): 780-920nm), flown at an average aircraft altitude of 2,205m. The cameras have a large field of view (typically about 35 degrees from nadir) and so collect high spatial-resolution data from relatively low altitudes with large aerial coverage. The average ground spatial resolution of the imagery is 1-meter. Imagery was acquired in 1,000 x 1,500 m frames with 35% side- and end-lap, and the frames were mosaicked and georeferenced, all by a private consultant (Positive Systems Inc. of Montana). More information about the imagery can be found in Kelly (2003) and Kelly et al (In press).

A subset image of 800 X 800 pixels was clipped from the mosaicked image for each year: this area has moderate terrain variation, and includes forested and non-forested areas. The two images show complex local geometric deformation due to the following reasons: 1) difference in the viewing angle, 2) variation of the terrain, and 3) error propagation in the georeferencing and mosaicking processes. The near-infrared band of each image was used for control point extraction because the study area is highly vegetated and the near-infrared band provides the best contrast between vegetation and other land covers (Cole-Rhodes et al, 2003).

2.2 Control Point Extraction: Similarity Measures

The area-based method for control point extraction seeks to maximize some predefined objective functions. The basic assumption of these methods is that the objective functions are maximized at the position where two sub-images are correctly aligned. For area-based methods, similarity between two sub-images is often used to define the objective functions; therefore, appropriate similarity metrics are crucial to the extraction of high quality control points. Common similarity metrics used in image registration include sum of absolute difference (SSD), normalized cross-correlation (NCC), correlation coefficient (CC), and mutual information (MI). The definitions and the properties of all the four similarity metrics are reviewed as follows.

SSD is defined as the squared Euclidean distance measure between two sub-images:

$$d^2(u, v) = \sum_x \sum_y [M(x, y) - S(x - u, y - v)]^2 \quad (1)$$

where M is the master image (or reference image by some authors) and S is the slave image (or input image by some authors); and the sum is over x, y of master sub-image under the window containing the slave sub-image positioned at u, v .

NCC metric is closely related to SSD by its formulation. In the expansion of d^2 , there are three terms involved:

$$d^2(u, v) = \sum_x \sum_y [M^2(x, y) - 2M(x, y)S(x - u, y - v) + S^2(x - u, y - v)] \quad (2)$$

The first term $M^2(x, y)$ is constant for a specific location (u, v) . The second term $M(x, y)S(x - u, y - v)$ is the sum of cross products, which can be taken as a kind of similarity measure. The last term $S^2(x - u, y - v)$ represents the local energy of slave sub-image centered at (u, v) , thus it's not constant and should be normalized. The NCC is then defined as the cross term normalized by the local energy:

$$NCC(u, v) = \frac{\sum_x \sum_y [M(x, y)S(x - u, y - v)]}{\sqrt{\sum_x \sum_y S^2(x - u, y - v)}} \quad (3)$$

CC is a pretty much standard statistics used in many similarity analyses. It treats two sub-images as two matrices of the same size and computes the two-dimensional correlation coefficient of two matrices. It is a statistical based similarity measure and ranges from -1 to 1 thus giving normalized similarity. It is calculated as

$$CC(u, v) = \frac{\sum_x \sum_y \{ [M(x, y) - \mu_M] [S(x - u, y - v) - \mu_S] \}}{\sqrt{\sum_x \sum_y [M(x, y) - \mu_M]^2} \sqrt{\sum_x \sum_y [S(x - u, y - v) - \mu_S]^2}} \quad (4)$$

where μ_M is the mean of master sub-image and μ_S is the mean of slave sub-image.

The above three similarity measures largely depend on the radiometric intensity of the target imagery, so they require images to be of the same nature and be radiometrically correlated. In addition, they are sensitive to certain amount of intensity changes between images. These

requirements limit their application on images from different sensors, different sensor capture characteristics (as with airborne imagery) and images with significant changes.

The fourth similarity measure discussed here, Mutual Information (MI) was first introduced to medical image registration (Viola et al, 1997; Collignon et al, 1995). Since then, it has become one of the favorite similarity measures for many researchers because of its superior performance. MI has its origin in information theory. It measures the statistical dependence or information redundancy of two random datasets. Unlike SSD, NCC and CC, MI does not assume the similar radiometric nature between two sub-images so it can be applied to multi-modal images with different radiometric properties and may be robust to a certain degree of changes (Chen, 2003).

Given master sub-image M and slave sub-image S, the mutual information between M and S can be equivalently defined in the following three equations:

$$I(M, S) = H(M) + H(S) - H(M, S) \quad (5)$$

$$I(M, S) = H(M) - H(M | S) \quad (6)$$

$$I(M, S) = H(S) - H(S | M) \quad (7)$$

where $H(M)$ and $H(S)$ are the entropies of M and S; $H(M, S)$ is the joint entropy of M and S; $H(M | S)$ and $H(S | M)$ are the conditional entropy of M given S and S given M. Denote $P_M(i)$ and $P_S(j)$ as the marginal probability distributions of M and S and $P_{M,S}(i, j)$ as the joint probability distribution of M and S, MI between M and S can be calculated from:

$$I(M, S) = \sum_i \sum_j P_{M,S}(i, j) * \log \left(\frac{P_{M,S}(i, j)}{P_M(i) * P_S(j)} \right) \quad (8)$$

To estimate MI between M and S based on (8), we only need to estimate the joint histogram between M and S, $h_{M,S}(i, j)$, from which all the terms in (8) can be

estimated: $P_M(i) = \frac{1}{N} \sum_j h_{M,S}(i, j)$, $P_S(j) = \frac{1}{N} \sum_i h_{M,S}(i, j)$, and $P_{M,S}(i, j) = \frac{1}{N} h_{M,S}(i, j)$, where N is the total number of pixels within each sub-images.

2.3 Control Point Extraction: Outlier Detection

Control points extracted by the aforementioned methods are not always meaningful and may contain outliers (Kennedy and Cohen, 2003). Spatial outliers are those spatial objects whose non-spatial attributes are significantly different from that of their spatial neighbors (Shekhar et. al. 2003). In this paper, I applied a spatial outlier detection method to screen those outliers. The simple z-score test was used to detect the control point outliers from the area-based methods. Z-score is defined as: $Z_i = \frac{(x_i - \bar{x}_i)}{\theta}$, where x_i is the testing spatial object, \bar{x}_i is the mean value of x_i 's neighbors, and θ is the standard deviation of x_i 's neighbors. When the absolute z value is great than a user predefined threshold, x_i is considered as an outlier. The threshold often ranges from 2 - 5. Attributes used in this study are the distance differences in x and y coordinates of a pair of control points in the master image and the slave image. I chose the distance differences in x and y coordinates instead of the absolute distance between the pair of control points because

the differences in x and y coordinates contain the information in both distance difference and direction difference. Therefore, the pair of control points is rejected if the distance difference in either x or y coordinate is found to be an outlier. In addition, defining the size of neighbor is another important part of the spatial outlier detection. If the size is too small, the method does not have enough points to ensure a robust estimation of z value; however, if the size is too large, the method is not able to capture the locally spatial variations of the attributes. In this study, I found that the 100m radius centered in the testing point was a suitable parameter and produce a satisfactory results in detecting outliers.

2.4 Transformation Model Determination

The transformation of the slave image coordinate system to the master image coordinate system follows the control point extraction from the image pairs. This process can be mathematically expressed by two sets of mapping functions with respect to two coordinate components of the master image. The coordinate mapping from any point $[u, v]$ in the slave image coordinate system to the corresponding point $[x, y]$ in the master image coordinate system is modeled as:

$$\begin{cases} x = f(u, v | \alpha) \\ y = g(u, v | \beta) \end{cases} \quad (9)$$

where α and β are parameters of the mapping function f and g respectively and are determined by control points, and are commonly determined by a global transformation.

There are many challenges presented by global transformations that require consideration here. For global transformation models such as affine transformation, projective transformation, and global polynomial transformation, the parameters α and β are the same for all the points and are determined by all the control points, so a single function is used to model the transformation for each component of coordinates. When the geometric distortion is complex and location dependent, global models become inadequate to model the image geometry. Linear functions such as affine transformation and projective transformation are too simple to take the local variation into consideration. Nonlinear functions such as global polynomials use the least square methods to optimize the parameters, thus the local variation will be averaged across the whole image (Zitova and Flusser, 2003; Goshtasby, 1988). Consequently, the registration error of locally deformed images by global functions is usually large and the spatial distribution of the error also varies with the location.

To solve these problems, local transformation models are proposed by Goshtasby (1986, 1987, 1988a 1988b) and Flusser (1992). A local transformation model seeks to decompose the entire image into pieces by triangulation, and then use different local mapping function to model the different local geometry for each piece. As a result, the parameters α and β vary across different local regions across the image and are significantly determined by the local control points. Common local transformation models include piecewise linear or nonlinear mapping functions and surface spline mapping functions. These models work well if sufficient evenly distributed control points are used. Therefore, the joint use of area-based methods for control point extraction with piecewise mapping functions for local geometric transformation as proposed in this paper is a promising approach for registration of airborne images with complex local deformation.

In this paper, I implemented the proposed image registration methods and conduct two types of comparisons: 1) different registration models: global models versus local models, and 2) different strategies for control point extraction: manual selection versus automatic area-based methods. For simplicity, I only compared two similarity measures CC and MI for control point extraction since SSD and NCC are similar to CC in principle. Specifically, the imagery from 2001 was transformed with respect to the image from 2000 by applying global transformation models (1st order and 2nd order polynomial functions) and local transformation models (piecewise linear and nonlinear mapping functions) with the control points by automatic area-based methods (CC and MI) and manual selection (MS). In total, I implemented 12 registrations from the combination of four geometric transformation models and three sets of control points.

3. Results

3.1 Parameter Determination

When area-based methods are applied to two images with a predefined window size on fixed grids, an appropriate window size should be determined so that it is large enough to be statistical significant and stable but as small as possible to minimize the local geometric variation within the image window. In addition, the spatial arrangement of the grids should be determined so that the resolution of the grids is fine enough to represent the geometric variation but as coarse as possible to minimize the computational requirement and regularize the overall distortion.

Preliminary exploration of the two images indicates that the possible maximum displacement would not exceed 25m, so 24 X 24 grids with 30m equal spacing are evenly arranged on the master image. The moving range of the slave image is thus specified as 25m in both row and column direction. Window sizes of 31, 41, 51, 61, 81, 101 were tested with each similarity measure on the ground truth points, and the size of 61 was proved to be optimal in the sense that 1) the curves of CC and MI are smooth and stable, 2) the peaks are sharp and unique, and 3) the window size is minimum for 1) and 2). Some examples on known control points are shown in figure 1, 2. The figures showed that the curves of CC and MI became more stable and robust when the window size increased to 61.

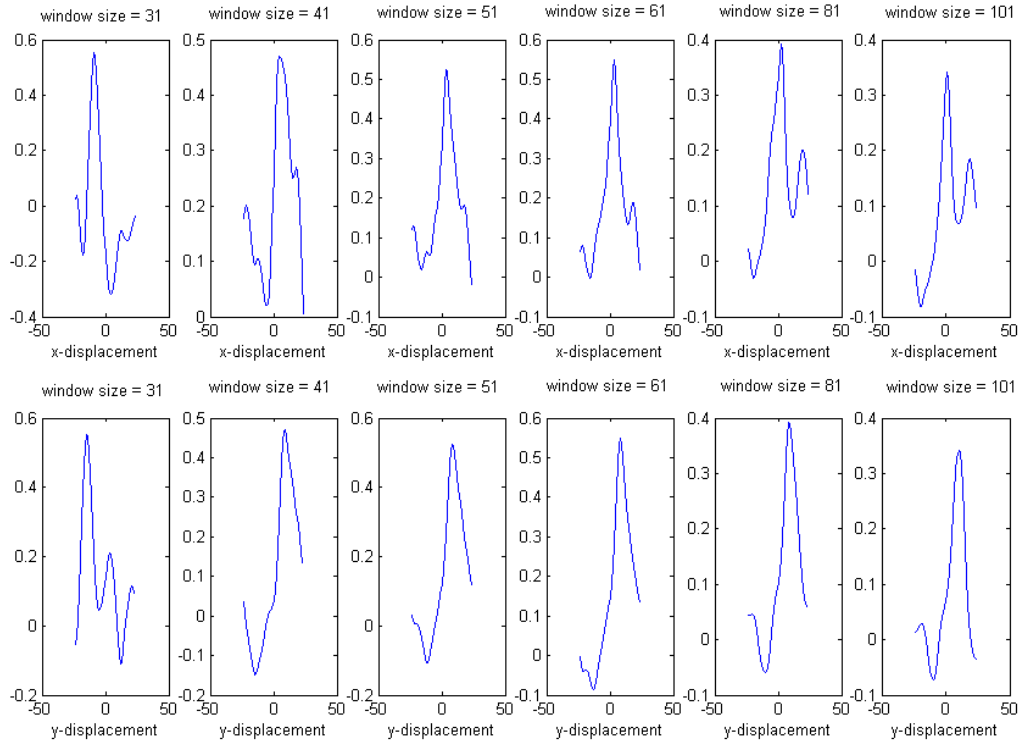


Figure 1. CC curves of displacement in x and y with different window size

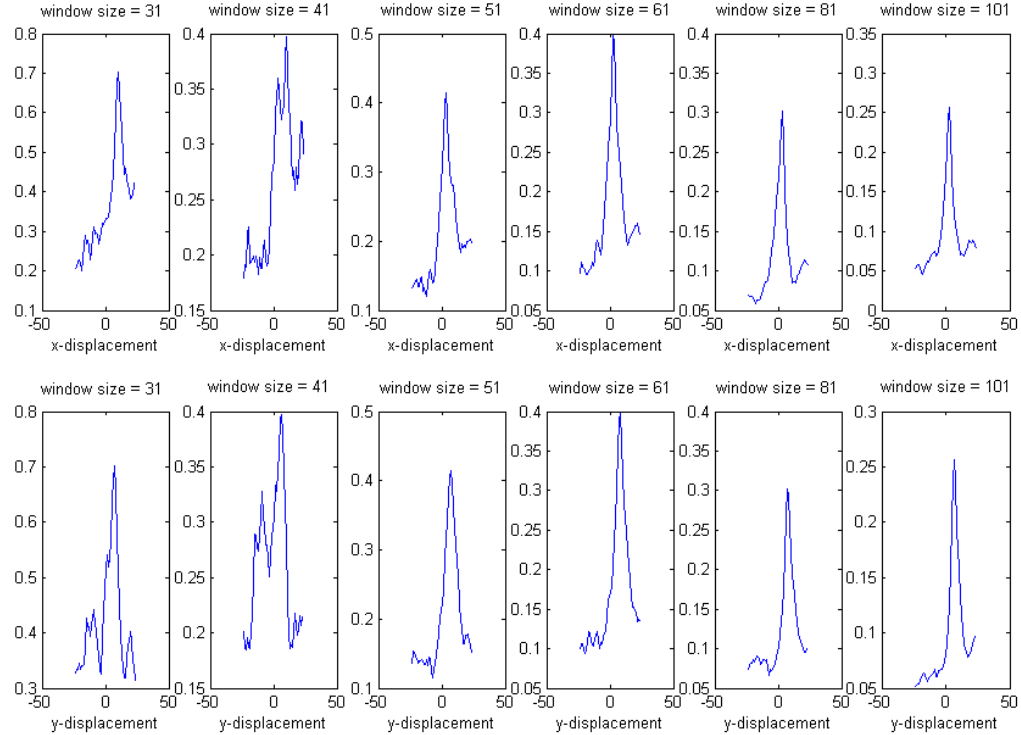


Figure 2. MI curves of displacement in x and y with different window size

3.2 Control Point Extraction

CC and MI were applied to the two images with the parameters determined in 3.1 (i.e. window size = 61m, range size=25, 24 X 24 grids of size 30m). The master image was the 61 X 61 sub-image of imagery 2000 centered on each grid. The slave image was the 61 X 61 sub-image of imagery 2001 with the center moving within the specified range of each grid. The control point at each grid was determined as the position where moving slave image maximizes the similarity measure. The maximum value was found by exhaustive search on the transformation space. To achieve sub-pixel level accuracy, spline-based interpolation on 0.2m X 0.2m grids was applied to a small area around the maximum value. The deformation vector plots for the two similarity measures are shown in figure 3 and figure 4.

The visualization of deformation vectors successfully represented the local details of image distortion. The plots of CC and MI showed similar spatial pattern of deformation vectors: the lower diagonal regions of the images were mismatched by more locally complex and irregular forces whereas the upper diagonal regions looked more smooth and regular. This is in accordance with the preliminary observation of the complex local geometric deformation. The upper left side of the image showed the image of 2001 shifted to left a lot with respect to the image of 2000, which is due to the error propagation of mosaicking and georeferencing between the two images. Moreover, a certain number of control point outliers were observed in the two deformation vector plots. Since the image deformation is assumed locally smooth and continuous, the outliers are detected as those deformation vectors differing much to their spatial neighbors in both direction and amplitude. The outliers detected by z-score test are shown as red dots on deformation vector plots in figure 3 and figure 4.

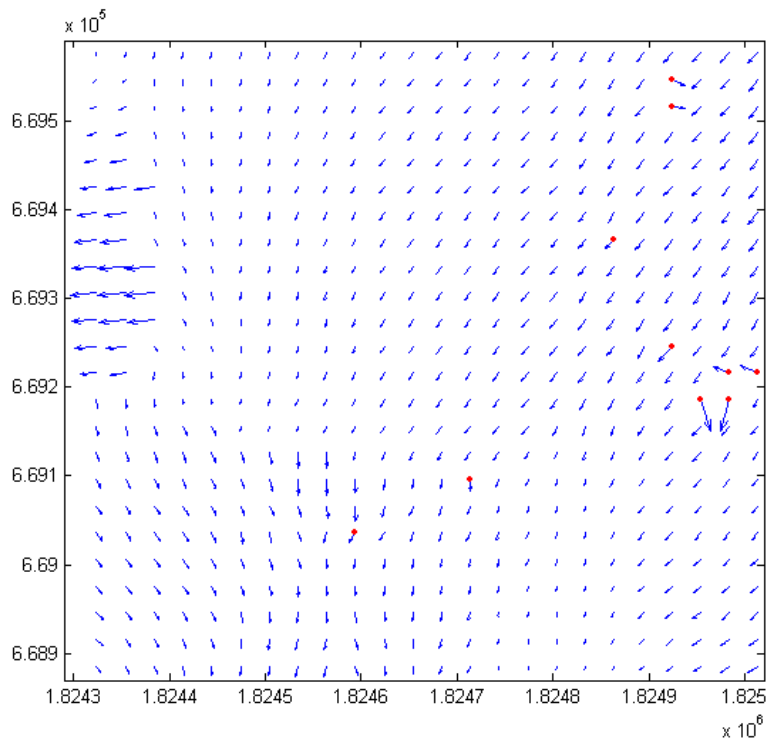


Figure 3. Deformation vector plot for CC

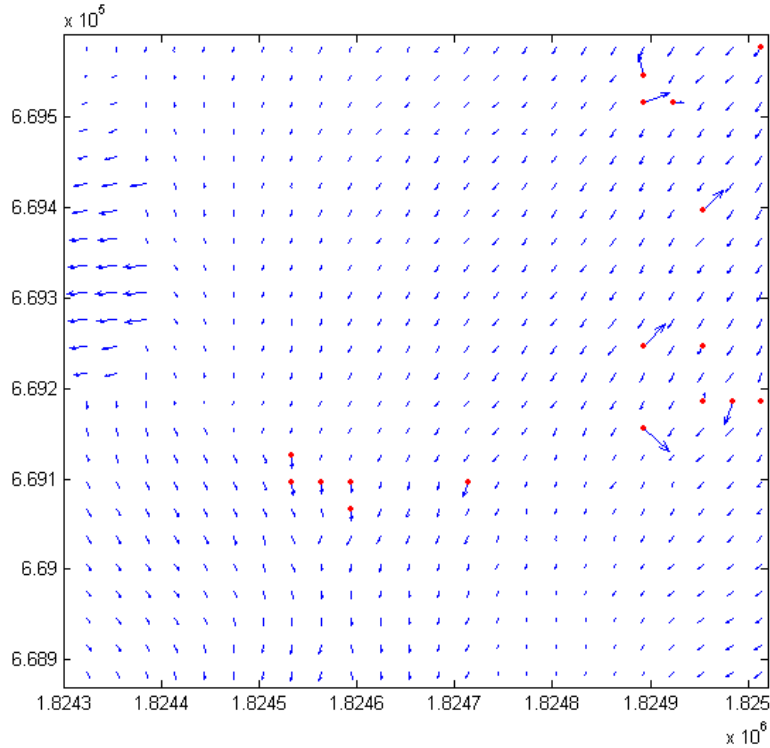


Figure 4. Deformation vector plot for MI

3.3 Transformation Models

Image of 2001 was transformed with respect to image of 2000 by applying piecewise linear and nonlinear models with the control points extracted from 3.2. First order and second order global polynomial models were also applied for the purpose of comparison. The control points were split randomly into two sets: one set for control, the other set for check. For CC, 400 control points were used to determine the model parameters and 166 independent check points were used to evaluate the registration accuracy. For MI, 400 control points and 159 independent check points were used. Since the amount of control points from manual selection is usually small compared to the automatic area-based methods and the precision of the control points is usually at the pixel level, it is readily expected that the proposed method will generate higher registration accuracy than manual method in terms of more accurate control points. To compare the difference of the control points from automatic methods with the manual selection for image registration, I also simulated the control points from the manual selection (MS) by only using 30 of the same 400 control points from CC for parameter estimation and the same 166 check points from CC for accuracy assessment. In addition, the coordinates of the control points were rounded off to the pixel level precision.

Root mean squared errors (RMSE) in x-direction, y-direction and both directions were calculated as a measure of the registration accuracy. In addition, the maximum residual in each direction and the standard deviation (SD) of the residuals were also calculated for the analysis of the error pattern. The piecewise linear and nonlinear models were implemented using the linear and

nonlinear rubber sheeting models in ERDAS Imagine. The statistics for accuracy assessment for CC, MI, and MS are reported in table 1.

Table 1. Accuracy assessment for CC, MI and MS

Control Point	Transformation Model	X RMSE	Max X Residual	Y RMSE	Max Y Residual	Total RMSE	SD of Residual
CC	P1	2.9116	18.962	1.5858	6.028	3.3154	1.660
	P2	3.0713	19.581	1.7124	5.273	3.5164	1.753
	PL	0.7459	3.248	0.5535	3.500	0.9288	0.469
	PN	0.7311	3.249	0.5308	3.383	0.9034	0.448
MI	P1	3.0368	19.365	1.5387	6.114	3.4044	1.685
	P2	3.0421	19.263	1.4523	5.276	3.3710	1.660
	PL	0.6612	4.038	0.6484	5.800	0.9260	0.469
	PN	0.6742	4.052	0.6284	5.459	0.9217	0.457
MS	P1	3.5671	15.555	1.6780	5.784	3.9421	2.404
	P2	4.9733	16.887	2.1266	5.460	5.4089	3.346
	PL	2.4326	10.699	1.3493	5.175	2.7818	1.965
	PN	2.4436	10.699	1.5100	5.175	2.8725	1.947
Note:	P1: 1 st order Polynomial		P2: 2 nd order Polynomial				
	PL: Piecewise Linear		PN: Piecewise Nonlinear				

For control points from CC, the local transformation models (piecewise linear and nonlinear functions) achieved sub-pixel accuracy whereas the total RMSEs for global models (1st and 2nd order global polynomial functions) are over 3 pixels. Moreover, the local models have much smaller maximum x-residual and maximum y-residual than the global models. This may be due to the fact that the global models lose the control for some specific distortions by averaging them across the whole image while local models can catch those local details. In addition, standard deviations of residuals for local models are much smaller than those for global models, which implies that the spatial errors of local functions are more evenly distributed than those of global functions which is varying across the whole image. The slight difference of linear and non-linear can be related to the amount of control points. Large amount of control points can decompose the whole image into many pieces so that non-linear distortion can be approximated by many pieces and linear function within each piece is enough to model the local distortion.

The same conclusions can also be found for the 4 registration models with control points from MI. MI is expected to be superior to CC in terms of more robustness to radiometric difference; however, very similar results was found between CC and MI for all models in table 1. This result can be explained by the differences in control points from CC and MI. The histogram (figure 5) of difference between control points from CC and MI shows that MI and CC agrees with each

other in most case and only very few difference exceeds 2m. The underlying reason may be that the multi-temporal images are from the same sensor (ADAR) and the radiometric correlation between two images is pretty good, thus MI didn't show its advantage over CC in control point extraction.

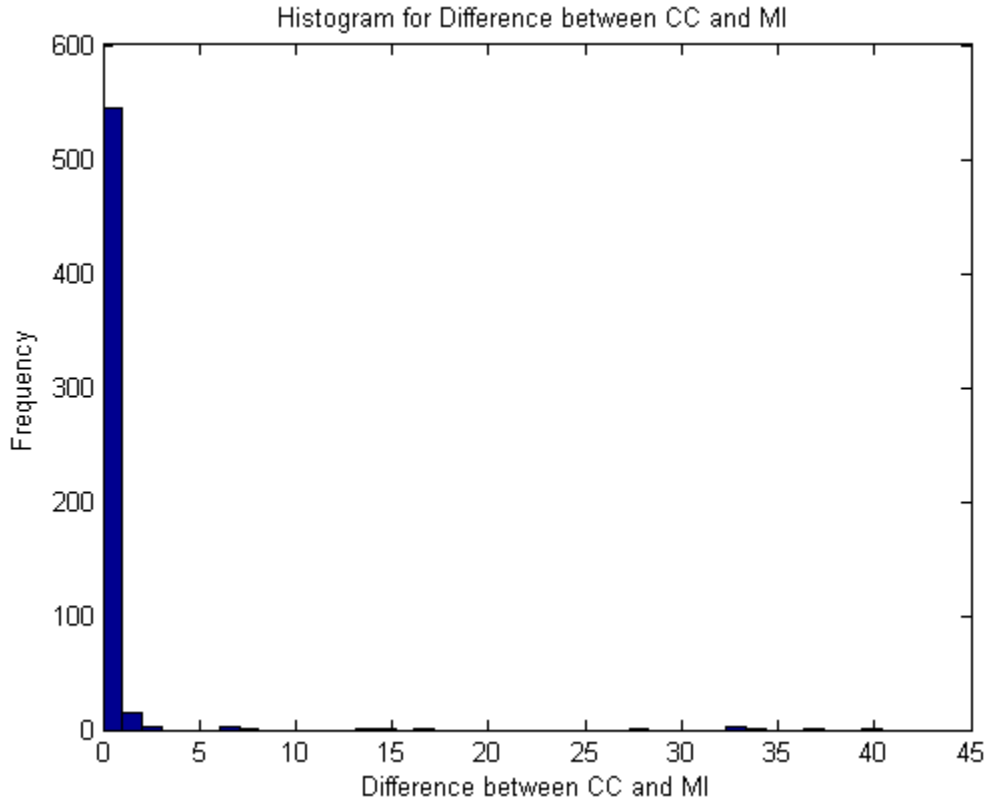


Figure 5. Histogram of difference between CC and MI

For control points from manual selection (MS), the local transformation models still outperformed global models in terms of the total RMSE, maximum x-residual, and maximum y-residual. In addition, standard deviations of residuals for local models are also smaller than those for global models. Comparing MS with CC and MI model by model, we can see that CC and MI achieved much lower registration error than MS for all the global models and local models. In particular, the total RMSE of two local models for MS are almost 3 times higher than those for CC and MI. This result indicates that larger amount of control points will improve the registration accuracy no matter global models or local models used. Therefore, local transformation models should work with more evenly distributed control points from automatic area-based methods in order to achieve higher registration accuracy.

4. Discussion and Conclusions

In this paper, I proposed an algorithm on automatic registration of two airborne images with complex local deformation by combining area-based control point extraction methods with local geometric transformation models. Two similarity measures (CC and MI) were used and

compared for the control point extraction. The area-based methods generated large amount of evenly distributed control points on regular grids. The control points with outliers removed were then applied to both global transformation models and local transformation models. Accuracy assessments showed that the local transformation models outperformed global transformation models in terms of total RMSE, standard deviation of residual, and maximum x-residual and y-residual. The difference in all the registration error statistics between CC and MI was slight, which may be due to the similar radiometric property between two images. CC works well for the same type of images whereas MI works better when multi-modal images are used.

To test the effect of quantity of control points on transformation models, another comparison was also performed between control points from automatic area-based methods and control points from manual selection. The results showed that control points from automatic area-based methods achieved much lower registration errors than control points from manual methods for all the global transformation models and local transformation models. This indicates that 1) more evenly distributed control points can better model the local distortion when local transformation models are used 2) more control points can reduce the expected prediction error (estimated by RMSE) and the variance of RMSE by the principle of least square methods when global transformation models are used.

In summary, the combination of area-based control point extraction with local transformation models is justified to be more appropriate for the geometric registration of airborne images with complex local distortion: 1) the area-based methods generated larger amount of evenly distributed control points compared to feature-based methods and manual methods; 2) local transformation models achieved better registration accuracy when larger amount of evenly distributed control points are used.

5. Acknowledgements

This research is supported by NASA Earth System Science graduate student fellowship to Desheng Liu.

6. References

- Brown, L. G., 1992. A survey of image registration techniques, *ACM Computing Surveys*, 24(4): 325-376.
- Chen, H.M., M. K. Arora, and P. K. Varshney, 2003. Mutual information-based image registration for remote sensing data, *International Journal of Remote Sensing*, 24(18): 3701-3706.
- Chen, H.M., P. K. Varshney, and M. K. Arora, 2003. Performance of mutual information similarity measure for registration of multitemporal remote sensing images, *IEEE Transaction on Geoscience and Remote Sensing*, 41(11): 2445-2454.

Cole-Rhodes, A.A., K. L. Johnson, J. L. Moigne, and I. Zavorin, 2003. Multiresolution registration of remote sensing imagery by optimization of mutual information using a stochastic gradient, *IEEE Transaction on Image Processing*, 12(12): 1495-1511.

Collignon, A., F. Maes, D. Delaere, D. Vandermeulen, P. Suetens, and G. Marchal, 1995. Automated multi-modality image registration based on information theory, *Information Processing in Medical Imaging*, Norwell, MA: Kluwer, 263-274.

Coulter, L. L., D. A. Stow, and S. Baer, 2003, A frame center matching technique for precise registration of multitemporal airborne frame imagery, *IEEE Transaction on Geoscience and Remote Sensing*, 41(11): 2436-2444.

Dai, X. and S. Khorram, 1998, The effects of image misregistration on the accuracy of remotely sensed change detection, *IEEE Transaction on Geoscience and Remote Sensing*, 36(5): 1566-1577.

Devereux, B.J., R.M. Fuller, L. Carter, and R.J. Parsell, 1990. Geometric correction of airborne scanner imagery by matching delaunay triangles, *International Journal of Remote Sensing*, 11(12): 2237-2251.

Flusser, J., 1992. An adaptive method for image registration, *Pattern Recognition*, 25(1): 45-54.

Fonseca, L. M.G. and B.S. Manjunath, 1996. Registration techniques for multisensor remotely sensed imagery, *Photogrammetric Engineering & Remote Sensing*, 62(9): 1049-1056.

Goshtasby, A., 1986. Piecewise linear mapping functions for image registration. *Pattern Recognition*, 19(6): 459-466.

Goshtasby, A., 1987. Piecewise cubic mapping functions for image registration, *Pattern Recognition*, 20(5): 525-533.

Goshtasby, A., 1988a. Registration of images with geometric distortions, *IEEE Transaction on Geoscience and Remote Sensing*, 26(1): 60-64.

Goshtasby, A., 1988b. Image Registration by Local Approximation Methods, *Image and Vision Computing*, 6(4): 255-261.

Jensen, J. R., 2004. *Introductory digital image processing*, 3rd Ed., Upper Saddle River, NJ: Prentice Hall.

Kelly, M., D. Shaari, Q. Guo, and D. Liu. A comparison of standard and hybrid classifier methods for mapping hardwood mortality in areas affected by sudden oak death. Accepted for publication in *Photogrammetric Engineering and Remote Sensing*.

Kelly, M. 2003. Remote sensing of sudden oak death using ADAR imagery. *Proceedings of the Ninth Forest Service Remote Sensing Applications Conference "Rapid Delivery of Remote*

Sensing Products". April 8-12, 2002. San Diego, CA. American Society for Photogrammetry and Remote Sensing.

Kennedy, R.E. and W.B. Cohen, 2003, Automated designation of tie-points for image-to-image coregistration, *International Journal of Remote Sensing*, 24(17): 3467-3490.

Moigne, J. L., W. J. Campbell, and R. F. Crompton, 2002, An automated parallel image registration technique based on the correlation of wavelet features, *IEEE Transaction on Geoscience and Remote Sensing*, 40(8): 1849-1864.

Richards, J.A. and X. Jia, 1999. *Remote sensing digital image analysis: an introduction*, 3rd edition. New York: Springer-Verlag.

Schowengerdt, R. A., 1997, *Remote sensing: models and methods for image processing*, 2nd edition. San Diego: Academic Press.

Shekhar, S., C. Lu, and P. Zhang, 2003. A unified approach to detecting spatial outliers, *Geoinformatica*, 7(2): 139-166.

Townshend, J.R.G., C.O. Justice, C. Gurney, and J. McManus, 1992. The impact of misregistration on change detection. *IEEE Transaction on Geoscience and Remote Sensing*, 30(5): 1054-1060.

Viola, P. and W. M. Wells III, 1997, Alignment by maximization of mutual information, *International Journal of Computer Vision*, 24(2): 137-154.

Zitova, B. and J. Flusser, 2003, Image registration methods: a survey, *Image and Vision Computing*, 21(11): 977-1000.